

# Learning from deep learning: better cosmological parameter inference from weak lensing maps

Dezső Ribli<sup>1</sup>, Bálint Ármin Pataki<sup>1</sup>, and István Csabai<sup>1\*</sup>

<sup>1</sup>Department of Physics of Complex Systems, Eötvös Loránd University,  
Budapest

\*csabai@complex.elte.hu

December 13, 2021

## Abstract

Gravitational weak lensing is one of the most promising probes of cosmology. Due to nonlinearities on small scales, the traditional analysis with two-point statistics does not fully capture all the underlying information [1]. Multiple inference methods were proposed to extract more details based on higher order statistics [2], peak statistics [3–5], Minkowski functionals [6, 7] and recently convolutional neural networks (CNN) [8]. Here we present an improved CNN that gives significantly better estimates of  $\Omega_m$  and  $\sigma_8$  cosmological parameters from simulated convergence maps than the state of art methods and also is free of systematic bias. Going beyond 'black box' style predictions, the investigation of the features learned by a high performing CNN revealed interesting insights. Without direct human assistance, only from the training data, the CNN discovered two familiar convolutional operators: the discrete Laplace operator and a Roberts cross kernel, which both characterize the steepness of the peaks. Using this insight we constructed a new, easy-to-understand, and robust peak counting algorithm which uses these operators, instead of the heights of the peaks. The new scheme significantly reduced prediction errors, and turned out to be even more accurate than the neural network.

## 1 Introduction

According to the standard cosmological model the initial small matter fluctuations evolved through gravitational collapse to yield the large scale structure of the current universe. This nonlinear physical process is sensitive to the model's parameters, such as the amplitude of the primordial density fluctuations ( $\sigma_8$ ) or the dark and baryonic matter content ( $\Omega_m$ ). One of the central questions of modern cosmology is to recover the precise values of cosmological parameters from observations however, due to the complexity and nonlinearity of the processes this inversion is a nontrivial task.

Dark matter cannot be observed directly but its weak gravitational lensing (WL) slightly distorts the apparent shapes of background galaxies. Several observational studies have measured this effect, and there are currently running, and planned efforts to provide even larger,

and higher resolution WL maps. The dark matter distribution inferred by WL maps can be then used to constrain parameters of cosmological models through analytical models or simulations [1].

Modern sophisticated n-body and hydrodynamical simulations [9] are able to reproduce the evolution of matter distribution and with ray tracing, simulated weak lensing maps can be produced [10]. These simulations aren't attempting to generate a particular realization of the universe that directly matches observations rather compliance of the model is usually measured by some derived statistical quantity.

Weak lensing is traditionally described by the two-point correlation function or the power spectrum, which are insensitive to the randomness of a particular realization, and fully characterize a homogeneous and isotropic Gaussian random field. However, on the small scales gravitational collapse distorts the Gaussian character of the initial fluctuations and two-point statistics are unable to capture all available information about the underlying cosmology [1]. In order to overcome this limitation, higher order statistics [11], peak statistics [12–14], Minkowski functionals [15] were used to extract the remaining, non-Gaussian information from weak lensing observations. Despite these efforts the  $(\Omega_m, \sigma_8)$  confidence areas from weak lensing are relatively large ( $\approx 1$ ) [13], and it was shown that neither the power spectrum, nor peak counting is able to accurately restore the planted parameters even from simulated high resolution noiseless weak lensing maps [8].

Convolutional neural networks have been shown to be able to extract very complex information from images and efficiently solve nonlinear inverse problems. Deep learning revolutionized computer vision in the past 6 years, it became the state of the art in virtually all computer vision tasks: image recognition, detection and segmentation. CNN-s have reached human accuracy and reduced error rates more than 10 fold in image recognition compared to previous approaches [16–19]. The ability of CNN-s to extract information from images, by learning from large amounts of labeled data, without explicit feature design, makes them attractive for various physical problems too, where hand crafted descriptors are used to analyze image data. CNNs have already been used in some astronomical and cosmological studies [8, 20] and they most probably have a vast unexploited potential.

## 2 Results

### 2.1 Improved CNN predictions

Following the idea and using the simulation data from a recent study [8] we created an improved CNN architecture (see details in the Methods) which is able to recover cosmological parameters more accurately from simulated weak lensing maps. The modifications mostly consisted of adding further activations, increasing the number of filters, and introducing a regular block structure. The input of the network is a set of mock convergence ( $\kappa$ ) maps generated by ray-tracing n-body simulations with 96 different values for the matter density  $\Omega_m$  and the scale of the initial perturbations normalized at the late Universe,  $\sigma_8$  (see [8] and [21] for details of the weak lensing map generation), the outputs of the network were the predicted cosmological parameters.

Our CNN's parameter estimation accuracy - on previously unseen lensing maps - beats all the state-of-art approaches for the complete parameter range and more importantly, it is free of systematic bias as shown in [Fig. 1] and summarized in [Table 1]. The CNN architecture used in the previous work [8] shows large errors, and strong bias in the predicted parameters, even close to the fiducial values. The improved CNN architecture predicts both  $\Omega_m$  and  $\sigma_8$  parameters with  $\approx 2\times$  smaller errors than peak counting in the full parameter range, with no

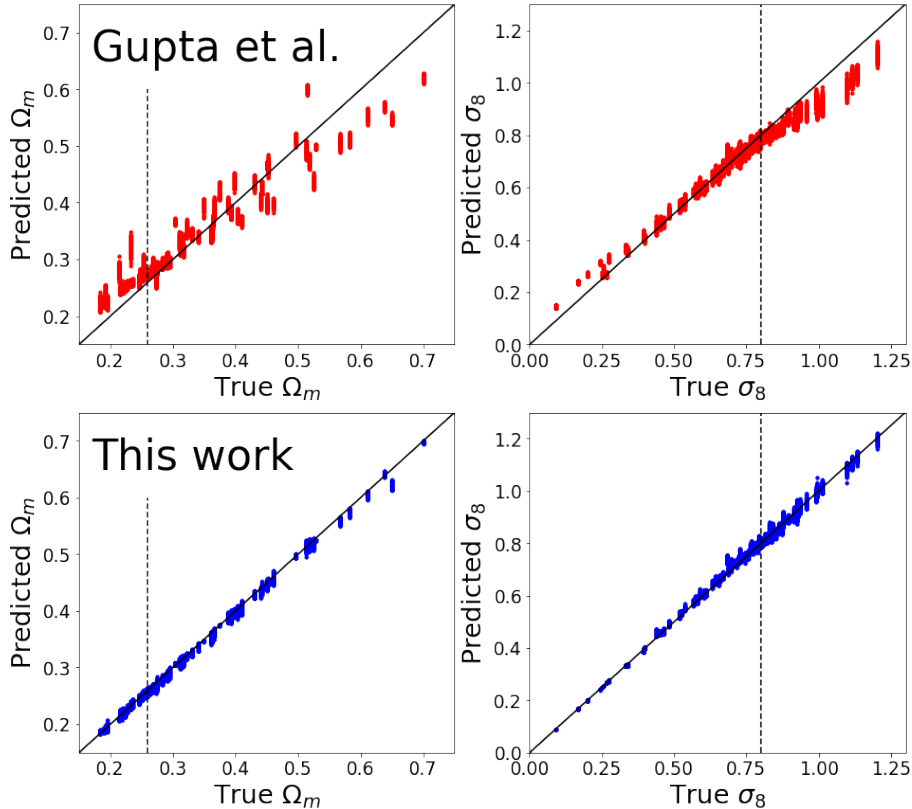


Figure 1: Neural network predictions vs. true cosmological parameters used in the simulations. Our CNN (bottom) shows significantly higher accuracy for both  $\Omega_m$  and  $\sigma_8$  parameters than the architecture from previous work [8] (top), and it also is free of strong systematic bias. The dashed lines mark the fiducial parameter values ( $\Omega_m = 0.26$ ,  $\sigma_8 = 0.8$ ).

bias, demonstrating that convolutional neural networks are indeed capable of extracting more information from weak lensing maps, than standard approaches.

Despite this superb performance there are caveats concerning the direct application of a CNN on real observations, when it had been trained on simulated data. A frequent objection against neural network models is that they are *black boxes* and without understanding the details of their decision process we cannot trust their results. A CNN has millions of parameters, and as shown in everyday image recognition tasks, it can be extremely sensitive to details of information in the images [22]. Even slight systematic differences between simulated maps and measurements might significantly bias the predictions of the neural network in an unpredictable manner.

## 2.2 Interrogating the neural network

While the complex interplay of millions of parameters simply cannot be fully comprehended, through careful investigation of the internal parameters of the trained neural network, we can gain insights into its workings. The internal representations of neural networks often have human-understandable interpretations, like legs of wheels of faces [23]. We have attempted to go even further, and not only to find these meaningful internal representations but to use them as a hint, and build an easy-to-understand and robust estimation method. In order to make the interpretation of the CNN’s weights easier, we trained a network with a  $7 \times 7$  kernel size in the first layer, on lensing maps resized to 2 arcmin pixel size, similar to the resolution expected from real observations. The inspection of the kernels immediately revealed that the neural

network discovered some interesting and familiar concepts [Fig 2], from the training data.

The neural network learned to use a kernel strikingly similar to a 2D discrete (negative) Laplace operator, that basically calculates the difference of the peaks and the surrounding pixel values. With the middle element scaled to 1 the learned kernel is the following:

$$K \approx \begin{bmatrix} -0.05 & -0.25 & -0.06 \\ -0.21 & 1 & -0.29 \\ -0.07 & -0.15 & -0.22 \end{bmatrix} \quad (1)$$

Using this hint, we considered the most isotropic discrete Laplace operator [24], which is very close to the learned kernel, and a simpler version with zeros in the corners.

$$L_1 = \frac{-10}{3} \begin{bmatrix} -0.05 & -0.2 & -0.05 \\ -0.2 & 1 & -0.2 \\ -0.05 & -0.2 & -0.05 \end{bmatrix}, L_2 = -4 \begin{bmatrix} 0 & -0.25 & 0 \\ -0.25 & 1 & -0.25 \\ 0 & -0.25 & 0 \end{bmatrix} \quad (2)$$

Another interesting kernel learned by the neural network is very similar to a Roberts cross kernel [Fig 2], which approximates the gradient of an image [25]:

$$R_x = \begin{bmatrix} 0 & 1 \\ -1 & 0 \end{bmatrix}, R_y = \begin{bmatrix} 1 & 0 \\ 0 & -1 \end{bmatrix}, \nabla I = \sqrt{G_x^2 + G_y^2}, \quad (3)$$

where the Roberts cross kernels are denoted by  $R_x, R_y$ , the computed gradients with  $G_x, G_y$  and the magnitude of the gradient with  $\nabla I$ .

Kernels (2)-(3) calculate the difference of peak values and their surrounding, or the gradients around a peak, therefore they potentially describe the steepness of peaks. As steeper peaks are also higher, steepness is strongly correlated with the height of the peaks, that are used in the standard peak counting method for parameter estimation in weak lensing, but it may contain more information than height. A previous study has shown that  $\Omega_m$  and  $\sigma_8$  cosmological parameters have substantial effect on the stacked tangential shear profile of peaks, and their steepness [5], which may explain why these kernels were discovered and used by the neural network.

### 2.3 Learning from deep learning: a simple descriptor using peak steepness

Based on these insights we can conclude that the neural network achieves better results than peak counting in part by using representations based on the steepness of the peaks. Beyond understanding the success of the CNN, the steepness of peaks can be used as a simple and robust descriptor, without the rest of the network and its countless other parameters. With the kernels (2)-(3) learned from the CNN we created a new algorithm that use the distribution of peak steepness values instead of the peak heights, which is used in the original scheme.

The results achieved with the new peak counting scheme are shown on [Fig 2], and summarized in Table 1. Using the kernels suggested by the CNN prediction errors were reduced over 2 fold for both  $\Omega_m$  and  $\sigma_8$  parameters compared to the original peak counting algorithm. Another rather surprising result is that the new peak counting scheme even surpassed the neural network's performance. The accurate results indicate that the kernels extracted from the neural network were indeed responsible for its high accuracy, and it was possible to combine the best of both approaches in the new peak counting method.

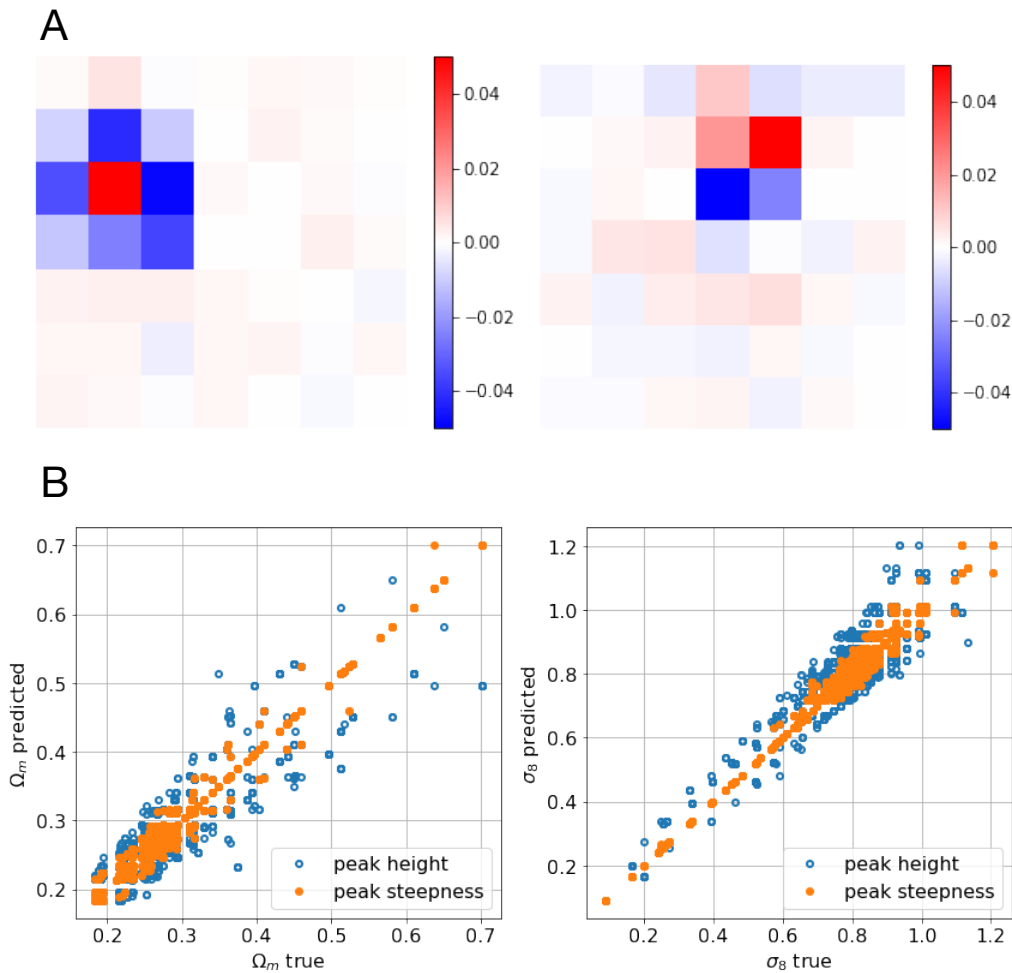


Figure 2: A: The two most characteristic kernels in the first layer of the CNN, the (negative) discrete Laplace operator (left), and a Roberts cross kernel (right). B: Predictions and true cosmological parameter values used in the simulations and with the original and the new peak counting schemes. Peak steepness is only shown with the Roberts cross kernel, which has the highest accuracy. The smaller scatter of the predictions show that the new peak counting scheme has higher accuracy. The results were calculated on the original 0.2 arcmin resolution, noiseless, simulated convergence maps.

	$\Omega_m$ (RMSE) $\times 10^3$	$\sigma_8$ (RMSE) $\times 10^3$
Peak counting	11.2	22.8
CNN [8]	35.1	40.3
CNN (ours)	5.5	13.5
Laplace v1	4.7	11.6
Laplace v2	4.6	10.9
Roberts cross	<b>4.3</b>	<b>9.7</b>

Table 1: Overview of prediction errors for CNN and peak counting schemes.

In order to gain some insight into the mechanism of the new peak counting, we show the mean histograms of the peak heights, and the steepness values for 4 simulations with different  $\Omega_m$ , but similar  $\sigma_8$  parameters, [Fig.3]. The distribution of steepness values seem to change similarly to peak height with different  $\Omega_m$  values, but the separation of the curves is larger for low and intermediate values, which potentially explain the better discrimination. Similar effects appear on the histograms when changing  $\sigma_8$  values.

We calculated the effect of each histogram bin on the parameter discrimination ability around the fiducial parameters using a  $\chi^2$  value, assuming uncorrelated errors,  $\chi_{bin}^2 = (y_{bin} - \mu_{bin})^2 / \sigma_{bin}^2$ . The  $\chi_{bin}^2$  value was calculated from the mean peak histograms, using the fiducial parameters ( $\Omega_m = 0.26, \sigma_8 = 0.8$ ) as 'model' and a very close parameter set ( $\Omega_m = 0.268, \sigma_8 = 0.801$ ) as the 'measurement'. The overall  $\chi_{bin}^2$  value is larger in the case of peak steepness, indicating better discrimination between the two set of parameters, and the bins with low and intermediate values have the largest contribution [Fig.3].

The weak lensing maps used in this study have a very high angular resolution (0.2 arcmin), which is not reachable in experiments. LSST is expected to produce lensing maps with an angular resolution of 1 arcmin [26], and the currently available CFHTLenS data has similar resolution [13, 27], therefore we evaluated the reconstruction errors on maps with reduced angular resolutions [Fig 3]. The new peak counting scheme based on steepness continues to predict  $\Omega_m$  and  $\sigma_8$  parameters more accurately than peak height at lower angular resolutions too. The results indicate that the steepness of the lensing map around peaks contain additional information compared to the height of the peaks, even for extended distances.

### 3 Discussion

Deep convolutional neural networks are promising new tools for the analysis of 2 or 3 dimensional scientific datasets, and the adopters of this technology need to be aware that small details may create large differences in the quality of predictions. The complexity of choices make working with neural networks more like an art with no simple recipe for success.

'Black box'-like CNN models may not be appropriate for direct inference from measurement data, and we expect that our approach of building simple and robust descriptors based on the insights gained from interrogating a neural network may be applicable to other scientific machine learning studies.

Our results indicate that peak counting based on the steepness of peaks have the potential to tighten the constraints of both  $\Omega_m$  and  $\sigma_8$  cosmological parameters compared to established methods. Improved parameter constraints from future surveys could alleviate or strengthen the tension between estimates gained from local and cosmic microwave background measurements [28]. The proposed scheme's efficiency on measurement data and its susceptibility to noise needs to be assessed in a future study.

### 4 Methods

**Data:** Weak lensing convergence maps were generated with ray tracing from 96 cosmological N-body simulations, with 512 independent realizations from each simulation [8]. Individual simulations had different pairs of  $\Omega_m$  and  $\sigma_8$  cosmological parameters. The parameters were most densely sampled around a 'fiducial model' with ( $\Omega_m = 0.26, \sigma_8 = 0.8$ ), for more details see [8]. One of the simulations ( $\Omega_m = 0.285, \sigma_8 = 1.134$ ) was not used as it was an obvious outlier based on [8] and our findings too.

**Training neural networks:** The lensing maps were split into a training, validation and test set as 60%, 10% and 30%. Each  $1024 \times 1024$  pixel map was tiled into 16 smaller images. During training the network handled the tiles individually, and during prediction, the inferred values of the 16 tiles were averaged in order to obtain a final prediction for a whole map. The networks were trained for 5 epochs with Adam optimizer. The optimizer's parameters were  $lr = 10^{-4}, \beta_1 = 0.9, \beta_2 = 0.999$ . The loss was MSE (mean squared error) for the modified

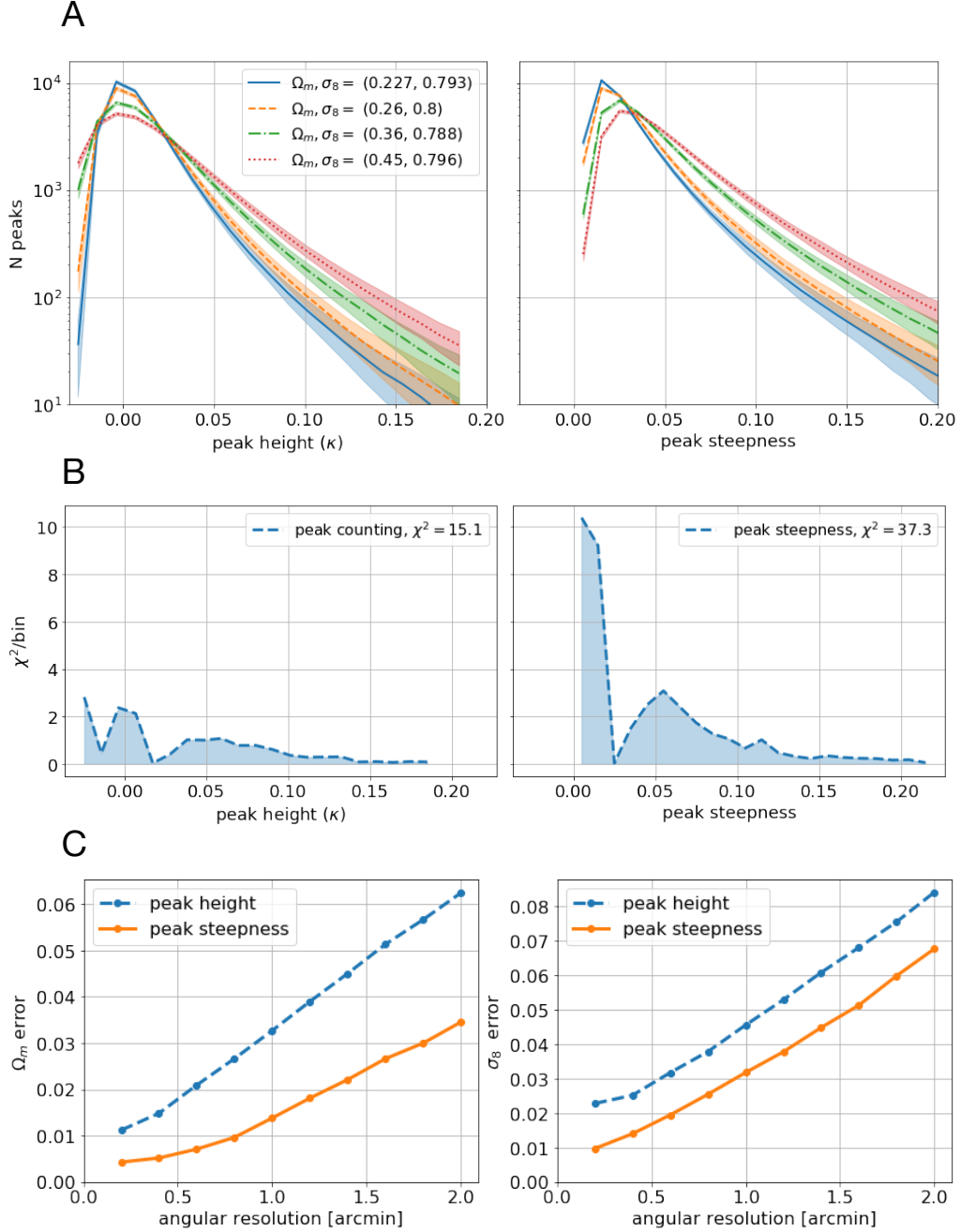


Figure 3: **A**: Peak counting height and a steepness distributions, and their sensitivity to  $\Omega_m$  parameter. Steepness values were calculated with the Roberts cross kernels. The mean counts are shown as the lines, and the colored area corresponds to  $2\sigma$  intervals. **B**: The distribution of  $\chi^2$  over the bins, when comparing histograms from two simulations: ( $\Omega_m = 0.268, \sigma_8 = 0.801$ ) as 'measurement' and ( $\Omega_m = 0.26, \sigma_8 = 0.8$ ) as the 'model' template. The higher  $\chi^2$  for peak steepness, indicates that it can discriminate the two pairs of parameters more accurately. Lower and intermediate value bins have the largest contribution. **C**: The effect of angular resolution on the errors of the different peak counting schemes. Peak steepness has higher accuracy at lower angular resolutions too.

architecture and MAE (mean absolute error) for the architecture from [8], as it was used in their analysis too.

**Improved neural network architecture:** Instead of building a neural network from

completely scratch, we decided to use the model from the previous work [8] as a starting point, in order to highlight the important differences which radically improve performance. The architectural guidelines were based on the work of very successful computer vision models [16, 17]. **A**, Firstly we made sure that each convolution is followed by an activation layer. **B**, Unusually low number of filters in the first layer might cause under-fitting, therefore we increased the number of filters in the first layer from 4 to 32. **B**, We introduced a regular block structure, made of subsequent 2 convolutions and a spatial down sampling operation, which is a common structure [16, 17]. Note that although our model starts with more filters, it has less parameters overall (2,649,088 vs 1,467,618), due to less extensive dense layers.

Apart from improvements of the architecture, we also decided to simplify the network, in order to show which features are not absolutely necessary for good performance. We changed the LeakyReLU operations to simpler ReLU operations. With the large amount of simulation data available we also decided to drop the Dropout layers from the network. Mean absolute error (MAE) loss function was also replaced by the more commonly used mean square error (MSE) cost function. Otherwise the network does not use more advanced concepts e.g.: residual connections [19] or inception modules [18], and we even opted to omit batch normalization for simplicity. The outline of the network is shown in Table 2.

#	Layers	Output size
1	Convolution* ( $3 \times 3$ )	$254 \times 254 \times 32$
2	Convolution* ( $3 \times 3$ )	$252 \times 252 \times 32$
3	Average Pooling ( $2 \times 2$ )	$126 \times 126 \times 32$
4	Convolution* ( $3 \times 3$ )	$124 \times 124 \times 64$
5	Convolution* ( $3 \times 3$ )	$122 \times 122 \times 64$
6	Average Pooling ( $2 \times 2$ )	$61 \times 61 \times 64$
7	Convolution* ( $3 \times 3$ )	$59 \times 59 \times 128$
8	Convolution* ( $3 \times 3$ )	$57 \times 57 \times 128$
9	Average Pooling ( $2 \times 2$ )	$28 \times 28 \times 128$
10	Convolution* ( $3 \times 3$ )	$26 \times 26 \times 128$
11	Convolution* ( $3 \times 3$ )	$24 \times 24 \times 128$
12	Average Pooling ( $2 \times 2$ )	$12 \times 12 \times 128$
13	Convolution* ( $3 \times 3$ )	$10 \times 10 \times 128$
14	Convolution* ( $3 \times 3$ )	$8 \times 8 \times 128$
15	Average Pooling ( $2 \times 2$ )	$4 \times 4 \times 128$
16	Dense*	256
17	Dense*	256
18	Dense	2

Table 2: Network architecture. Modified neural network. The marked (\*) layers are followed by ReLU activations. Loss function is mean squared error (MSE). Number of parameters: 1.467.618.

**Peak counting baseline:** We evaluated peak counting statistics on the same dataset similarly to [8]. Peaks were defined as local maxima on the lensing maps. For each map, histograms of peak  $\kappa$  values were counted in 0.01 wide bins from  $-0.03$  to  $0.19$ . Individual histograms were compared to the mean histograms from each simulation, and the parameters corresponding to the simulation with the lowest  $\chi$  value were selected as prediction values. Each realization was evaluated when creating the mean histograms and the covariance matrices. The  $\chi$  values were computed as the following:



$$\chi_{\Omega,\sigma}^2 = (\mathbf{y} - \boldsymbol{\mu}_{\Omega,\sigma}) \mathbf{C}_{\Omega,\sigma}^{-1} (\mathbf{y} - \boldsymbol{\mu}_{\Omega,\sigma}) \quad (4)$$

Where  $\mathbf{y}$  denotes the counts as a vector for a given map,  $\boldsymbol{\mu}$  the mean counts for a simulation, and  $\mathbf{C}$  the covariance matrix of the histograms for a given simulation. Note that the covariance matrix is calculated separately for each simulation, instead of using a fixed covariance which is calculated for a selected model as in [8]. In order to avoid problems when some simulations had no variance in some bins, we used the pseudo inverse of the covariance matrices instead of their inverse. The varying covariance matrix eliminates strong systematic errors when the covariance matrices of different simulations differ significantly. We verified that using a varying covariance instead of a fixed covariance the prediction errors of the peak counting approach were significantly reduced.

**Peak steepness counting:** The approach is almost the same as peak counting, but we use the histograms of the calculated steepness values, instead of the histograms of the peak height values. For the discrete Laplace filter the convolution is straightforward, in the case of the Roberts cross we found that the best results can be achieved if one calculates the sum of the magnitudes of the gradient in the 4 adjacent 2x2 blocks around the peak. One small difference compared to peak heights is that calculated values are positive by definition at the local peaks, therefore we adjusted bins to run from 0 to 0.22 for the new values. Otherwise the number and width of bins remained the same as for peak counting. We verified, that a similar bin shift for the original peak counting scheme does not explain the different results, and small differences in the bin width or the range do not noticeably alter the the results in either schemes.

**Reducing angular resolution:** When testing on lower angular resolutions, we resized the weak lensing maps to a resolution which is an integer times the original resolution, (1,2,3..). In this decimating scheme the new pixel values were calculated as the means of the pixel values in the area corresponding to the new pixel in order to avoid artifacts, like moiré in the low resolution maps. Reducing angular resolution this way does not destroy gradients like a Gaussian-blur used in [8], therefore the modified peak counting schemes can still work on reduced resolution maps. We expect that measurement data can be handled in a similar way, which does not destroy differences among neighboring pixels. The distribution of gradient values were observed to become larger at lower resolutions, therefore we increased the bin width linearly from 0.01 to 0.02, when changing resolution from 0.02 to 2.0 arcmins.

**Acknowledgements:** This work was partially supported by National Research, Development and Innovation Office of Hungary via grant OTKA NN 114560 and the National Quantum Technologies Program. The authors thank Z Haiman and JMZ Matilla for making available the simulated weak lensing maps used in this study.

## References

- [1] Martin Kilbinger. Cosmology with cosmic shear observations: a review. *Reports on Progress in Physics*, 78(8):086901, 2015.
- [2] Masahiro Takada and Bhuvnesh Jain. Three-point correlations in weak lensing surveys: model predictions and applications. *Monthly Notices of the Royal Astronomical Society*, 344(3):857–886, 2003.
- [3] JP Dietrich and Jan Hartlap. Cosmology with the shear-peak statistics. *Monthly Notices of the Royal Astronomical Society*, 402(2):1049–1058, 2010.

- [4] Jan M Kratochvil, Zoltán Haiman, and Morgan May. Probing cosmology with weak lensing peak counts. *Physical Review D*, 81(4):043519, 2010.
- [5] Laura Marian, Robert E Smith, Stefan Hilbert, and Peter Schneider. The cosmological information of shear peaks: beyond the abundance. *Monthly Notices of the Royal Astronomical Society*, 432(2):1338–1350, 2013.
- [6] Andrea Petri, Zoltán Haiman, Lam Hui, Morgan May, and Jan M Kratochvil. Cosmology with minkowski functionals and moments of the weak lensing convergence field. *Physical Review D*, 88(12):123002, 2013.
- [7] Jan M Kratochvil, Eugene A Lim, Sheng Wang, Zoltán Haiman, Morgan May, and Kevin Huffenberger. Probing cosmology with weak lensing minkowski functionals. *Physical Review D*, 85(10):103513, 2012.
- [8] Arushi Gupta, José Manuel Zorrilla Matilla, Daniel Hsu, and Zoltán Haiman. Non-gaussian information from weak lensing data via deep learning. *arXiv preprint arXiv:1802.01212*, 2018.
- [9] Annalisa Pillepich, Volker Springel, Dylan Nelson, Shy Genel, Jill Naiman, Rüdiger Pakmor, Lars Hernquist, Paul Torrey, Mark Vogelsberger, Rainer Weinberger, et al. Simulating galaxy formation with the illustris model. *Monthly Notices of the Royal Astronomical Society*, 473(3):4077–4106, 2017.
- [10] Chris Vale and Martin White. Simulating weak lensing by large-scale structure. *The Astrophysical Journal*, 592(2):699, 2003.
- [11] Liping Fu, Martin Kilbinger, Thomas Erben, Catherine Heymans, Hendrik Hildebrandt, Henk Hoekstra, Thomas D Kitching, Yannick Mellier, Lance Miller, Elisabetta Semboloni, et al. Cftlens: cosmological constraints from a combination of cosmic shear two-point and three-point correlations. *Monthly Notices of the Royal Astronomical Society*, 441(3):2725–2743, 2014.
- [12] HuanYuan Shan, Jean-Paul Kneib, Johan Comparat, Eric Jullo, Aldée Charbonnier, Thomas Erben, Martin Makler, Bruno Moraes, Ludovic Van Waerbeke, Frédéric Courbin, et al. Weak lensing mass map and peak statistics in canada–france–hawaii telescope stripe 82 survey. *Monthly Notices of the Royal Astronomical Society*, 442(3):2534–2542, 2014.
- [13] Jia Liu, Andrea Petri, Zoltán Haiman, Lam Hui, Jan M Kratochvil, and Morgan May. Cosmology constraints from the weak lensing peak counts and the power spectrum in cftlens data. *Physical Review D*, 91(6):063507, 2015.
- [14] Tomasz Kacprzak, D Kirk, O Friedrich, A Amara, A Refregier, L Marian, JP Dietrich, E Suchyta, J Aleksić, D Bacon, et al. Cosmology constraints from shear peak statistics in dark energy survey science verification data. *Monthly Notices of the Royal Astronomical Society*, 463(4):3653–3673, 2016.
- [15] Masato Shirasaki and Naoki Yoshida. Statistical and systematic errors in the measurement of weak-lensing minkowski functionals: application to the canada-france-hawaii lensing survey. *The Astrophysical Journal*, 786(1):43, 2014.
- [16] Alex Krizhevsky, Ilya Sutskever, and Geoffrey E Hinton. Imagenet classification with deep convolutional neural networks. In *Advances in neural information processing systems*, pages 1097–1105, 2012.

- [17] Karen Simonyan and Andrew Zisserman. Very deep convolutional networks for large-scale image recognition. *arXiv preprint arXiv:1409.1556*, 2014.
- [18] Christian Szegedy, Wei Liu, Yangqing Jia, Pierre Sermanet, Scott Reed, Dragomir Anguelov, Dumitru Erhan, Vincent Vanhoucke, Andrew Rabinovich, et al. Going deeper with convolutions. *Cvpr*, 2015.
- [19] Kaiming He, Xiangyu Zhang, Shaoqing Ren, and Jian Sun. Deep residual learning for image recognition. In *Proceedings of the IEEE conference on computer vision and pattern recognition*, pages 770–778, 2016.
- [20] Daniel George and EA Huerta. Deep neural networks to enable real-time multimessenger astrophysics. *Physical Review D*, 97(4):044039, 2018.
- [21] José Manuel Zorrilla Matilla, Zoltán Haiman, Daniel Hsu, Arushi Gupta, and Andrea Petri. Do dark matter halos explain lensing peaks? *Physical Review D*, 94(8):083506, 2016.
- [22] Christian Szegedy, Wojciech Zaremba, Ilya Sutskever, Joan Bruna, Dumitru Erhan, Ian Goodfellow, and Rob Fergus. Intriguing properties of neural networks. *arXiv preprint arXiv:1312.6199*, 2013.
- [23] Matthew D Zeiler and Rob Fergus. Visualizing and understanding convolutional networks. In *European conference on computer vision*, pages 818–833. Springer, 2014.
- [24] Tony Lindeberg. Scale-space for discrete signals. *IEEE transactions on pattern analysis and machine intelligence*, 12(3):234–254, 1990.
- [25] Lawrence G Roberts. *Machine perception of three-dimensional solids*. PhD thesis, Massachusetts Institute of Technology, 1963.
- [26] C Chang, M Jarvis, B Jain, SM Kahn, D Kirkby, A Connolly, S Krughoff, E-H Peng, and JR Peterson. The effective number density of galaxies for weak lensing measurements in the lsst project. *Monthly Notices of the Royal Astronomical Society*, 434(3):2121–2135, 2013.
- [27] Martin Kilbinger, Liping Fu, Catherine Heymans, Fergus Simpson, Jonathan Benjamin, Thomas Erben, Joachim Harnois-Déraps, Henk Hoekstra, Hendrik Hildebrandt, Thomas D Kitching, et al. Cfhtlens: combined probe cosmological model comparison using 2d weak gravitational lensing. *Monthly Notices of the Royal Astronomical Society*, 430(3):2200–2220, 2013.
- [28] Niall MacCrann, Joe Zuntz, Sarah Bridle, Bhuvnesh Jain, and Matthew R Becker. Cosmic discordance: Are planck cmb and cfhtlens weak lensing measurements out of tune? *Monthly Notices of the Royal Astronomical Society*, 451(3):2877–2888, 2015.